Path-dependent human identification using a pyroelectric infrared sensor and Fresnel lens arrays

Jian-Shuen Fang[1], Qi Hao[2], David J. Brady[2], Mohan Shankar[2], Bob D. Guenther[2], Nikos P. Pitsianis[2], Ken Y. Hsu[1]

[1] Department of Photonics & Institute of Electro-Optical Engineering, National Chiao Tung University, 1001 Ta Hsueh Rd., Hsinchu 300, Taiwan
[2] Fitzpatrick Center for Photonic and Communications, Duke University, Durham, NC 27707 USA
jsf.eo91g@nctu.edu.tw

Abstract: This paper presents a design and development of a low power consumption, and low cost, human identification system using a pyroelectric infrared (PIR) sensor whose visibility is modulated by a Fresnel lens array. The optimal element number of the lens array for the identification system was investigated and the experimental results suggest that the lens array with more elements can yield a better performance in terms of identification and false alarm rates. The other parameters of the system configuration such as the height of sensor location and sensor-to-object distance were also studied to improve spectral distinctions among sensory data of human objects. The identification process consists of two parts: training and testing. For the data training, we employed a principal components regression (PCR) method to cluster data with respect to different registered objects at different speed levels. The feature data of different objects walking along the same path in training yet at random speeds are then tested against the pre-trained clusters to decide whether the target is registered, and which member of the registered group it is.

OCIS codes: (110.3080) Infrared Imaging Systems; (040.3060) Infrared Detectors

References and links

1. M. Planck, "On the law of distribution of energy in the normal spectrum," Annalen der Physik **4**, 533 ff (1901).
2. V. Spitzer, M. Ackerman, A. Scherzinger, D. Whitlock, "The visible human male: A technical report," J. Am. Med. Assoc. **3**, 118-130 (1996).
3. N. Kakuta, S. Yokoyama, M. Nakamura, "Estimation of radiative heat transfer using a geometric human model," IEEE Trans. Biomed. Eng. **48**, 324-331 (2001).
4. Glolab Corporation, "Infrared parts manual," http://www.glolab.com/pirparts/infrared.html.
5. U. Gopinathan, D. J. Brady, N. P. Pitsianis, "Coded apertures for efficient pyroelectric motion tracking," Opt. Express. **11**, 2142-2152 (2003), http://www.opticsexpress.org/abstract.cfm?URI=OPEX-11-18-2142.
6. "A. S. Sekmen, M. Wilkes, and K. Kawamura, "An application of passive human-robot interaction: human tracking based on attention distraction," IEEE Trans. Syst., Man Cybern. A **32**, 248-259 (2002).
7. Q. Hao, D. J. Brady, B. D. Guenther, J. Burchett, M. Shankar, and S. Feller, "Human tracking with wireless distributed radial pyroelectric sensors," submitted to IEEE Sensors Journal.
8. Anil K. Jain, Arun Ross, Salil Prabhakar, "An introduction to biometric recognition," IEEE Trans. Circuits Syst. Video Technol. **14**, 4-20 (2004).
9. M. M. Trivedi, K. S. Huang, and I. Mikic, "Dynamic context capture and distributed video arrays for intelligent spaces," IEEE Trans. Syst., Man Cybern. A **35**, 145-163 (2005).
10. J. L. Geisheimer, W. S. Marshall, and E. Greneker, "A continuous-wave (CW) radar for gait analysis," Proc. of IEEE. Signals, Systems and Computers **1**, 843-838 (2001).
11. Fresnel Technologies Inc., http://www.fresneltech.com/arrays.html.

#9793 - $15.00 USD Received 30 November 2005; revised 17 January 2006; accepted 17 January 2006

1. Introduction

Human bodies are very good infrared sources. The temperature of a typical human body is about 37 ^{0}C or 98 ^{0}F. There is a constant heat exchange between the body and the environment due to the difference in their temperatures. The radiation characteristics of any object can be analyzed using the black-body radiation curve governed by Planck's Law [1]. For a typical human body, this curve is shown in Fig. 1. It can be seen that essentially all of the radiation is in the infrared region with the peak radiation occurring at 9.55 μm . To estimate human body radiation of heat to their environment, the Stefan-Boltzman's Law can be used [2]. The average human frame radiates about 100 W/m^2 of power [3]. Infrared detectors that are sensitive in a range of 8~14 μm would thus be able to detect humans within a fairly reasonable distance [4].

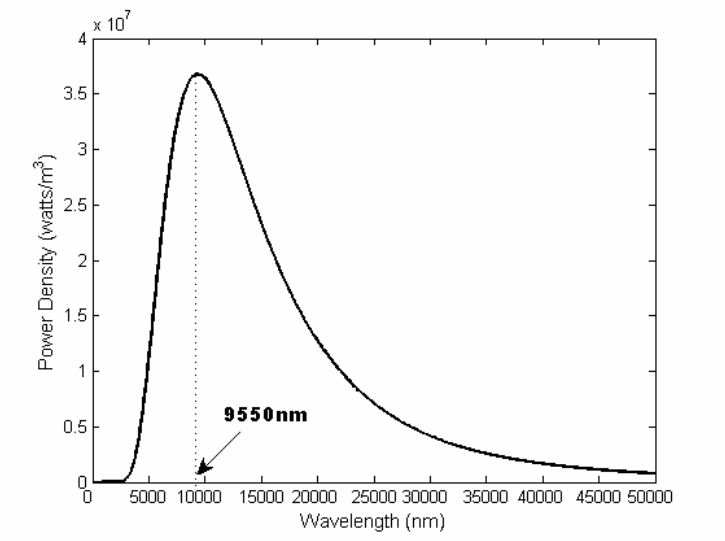

Fig. 1. Black-body radiation curve of human body at 37° C

The pyroelectric infrared (PIR) sensor has high performance for IR radiation detection at room temperature. Recently, PIR sensors have been used for a wide range of applications such as intruder detection, light actuators, and auxiliary sensing to complement the coverage of cameras [5, 6]. It turns out to be attractive for security applications due to its low cost, and low power consumption. Equally attractive, there is no need for special and expensive cooling. In [7], a wireless distributed pyroelectric sensor system has been described for human target tracking. However, not much attention has yet been said to another important aspect in human tracking: human identification. Indeed, human identification not only plays an important role in security systems and scene surveillance, but also is a necessity for tracking multiple humans, by reducing the mutual interference among those human objects during the tracking process.

A pyroelectric sensor system for human recognition can serve as a component of a biometric system, a requirement for many intelligent machine systems and secure systems. In conventional biometric systems, the complex structure of certain body parts, such as a human iris, human fingerprints, facial, or hand geometry, are measured optically, analyzed digitally, and a digital code is created for each person. When humans walk, the motion of various components of the body, including the torso, arms, and legs, produce a characteristic signature. Human walking motion is quite complex and it is rather difficult to decouple the individual biomechanical contributions of the motion cycle for analysis. Indeed, gait is not supposed to be very distinctive. Here we hope to demonstrate that it is sufficiently

#9793 - $15.00 USD Received 30 November 2005; revised 17 January 2006; accepted 17 January 2006

discriminatory to allow verification in some low-security applications. Much of the work on gait analysis as a behavior biometric has been conducted using video cameras which stream and process large amounts of data to extract the identity of the person under examination in a computationally expensive way [8, 9]. In [10], a continuous-wave (CW) radar has been developed to record the radar signature corresponding to the walking human gait.

From the thermal perspective, each person acts as a distributed infrared source whose distribution function is determined by their shape and the IR emission of their extremity. Combined with the idiosyncrasies in how they carry themselves, the heat will impact a surrounding sensor field in a unique way. By measuring the sensor response to a person in a prescribed walking path, we can map this response data to a code vector in a 2-D plane that unique identifies the person at a specific speed level.

A functional biometric system requires specific human characteristics in use to be [8]

1) Universal: each person should have his/her own characteristic;
2) Distinctive: any two persons should have separable characteristics;
3) Permanent: the characteristic should be sufficiently invariant, under a certain matching criterion, over a period of time;
4) Collectable: the characteristic must be a measurable quantity.

A biometric system is an intrinsic pattern recognition system and comprises three parts: feature representation, feature training (clustering), and feature testing [8]. In our study, data collected from a pyroelectric sensor was analyzed using spectral techniques to extract the motion features of individuals. The experimental results display the spectral distinctions among different humans walking at different speeds. The spectral features of objects at a specific speed can be collected repeatedly with small variances, given a fixed sensor configuration. By using the principal component regression (PCR) method, those spectral features can be clustered around a set of points, along a unit circle in a 2-D label plane. From the training process, we can obtain a regression vector locating a cluster, as well as the mean and covariance of a number of clusters. Then new data, of objects walking at random speeds, are used for testing the recognition capability.

The objective of this study is to explore the potential of using the pyroelectric IR sensor for security and human identification applications. The desired experimental results were obtained and show that the element number of Fresnel lens array, the height of sensor module and the distance between sensor and object impact identification performance.

2. Signal collection using a pyroelectric IR detector with Fresnel arrays

The pryoelectric IR detector used for this work is low cost, $ 2 per piece, and low power consumption, 2 mW. These detectors are available in single element or dual element versions. A single element detector responds to any temperature changes in the environment and therefore needs to be thermally compensated to remove sensitivity to ambient temperature. Dual element detectors have the inherent advantage that the output voltage is the difference between the voltages obtained from each of the elements of the detector which subtracts out environmental effect. The response of a dual element pyroelectric detector toward a point source is shown in Fig. 2, where the distance between the point source under testing and the sensor is normalized to show its generic visibility characteristic. Such a dual lobe visibility pattern is formed because the two pyroelectric elements are connected in series opposition. The signals obtained from each of the elements where a thermal source crosses the common area of overlap of the fields of view (FOVs) cancel one another.

#9793 - $15.00 USD Received 30 November 2005; revised 17 January 2006; accepted 17 January 2006

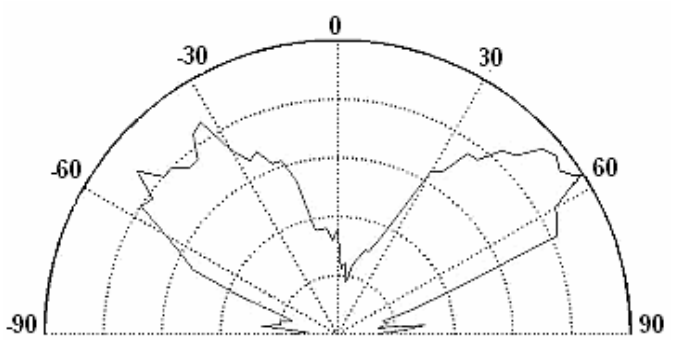

Fig. 2. Polar plot of response of the dual-element pyroelectric detector

In our system, we employ the dual element pyroelectric detector PIR325 from Glolab Corporation [4] to detect IR radiation from human bodies. The pyroelectric detectors have an angular visibility of over 100^0 but any motion near both the margins of FOV does not create a significant change in the thermal flux, resulting in very little response. The response of the detector depends on the incident power collected by the detector which in turn depends on the area of the detector. Since the detector elements have a small area ($2mm^2$), the amount of power collected is a very small fraction of the incident power.

To overcome this drawback, we used Fresnel lens to improve both the collection efficiency and spatial resolution. They can be molded out of inexpensive plastics with desired transmission characteristics (for the required wavelength range) making the system thin, light weight and inexpensive. In order to aid in the sensing of motion, Fresnel lens arrays are designed so that the visible space is divided into zones. Detection is enhanced by creating distinct regions of visibility. Each of the lenses on the array would typically create a single cone of visibility depending on the focal length and the size of the detector elements. However, with a dual element pyroelectric detector, the field of visibility of a lens is divided into two distinct zones, as illustrated in Fig. 3.

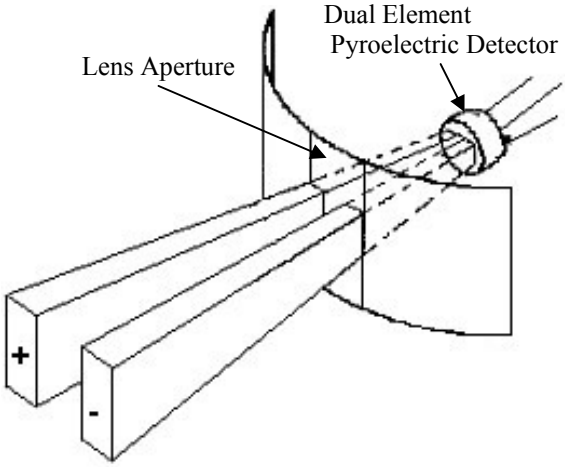

Fig. 3. Beams formed by a single lens on a lens array. The two beams correspond to each of the elements in a dual element detector.

We employ a commercially available lens array (Animal alley array- AA0.9GIT1) obtained from Fresnel Technologies Inc. [11]. The material of the lens has suitable transmission in the 8-14 μm . The FOV of lens array was characterized and illustrated in Fig. 4. A summary of the different parameters of this lens array is shown in Table 1. In this paper,

#9793 - $15.00 USD Received 30 November 2005; revised 17 January 2006; accepted 17 January 2006

we employed Fresenl lens arrays with 1, 3, 5, 9, 11 elements, modulated by the plastic masks shown in Fig. 5.

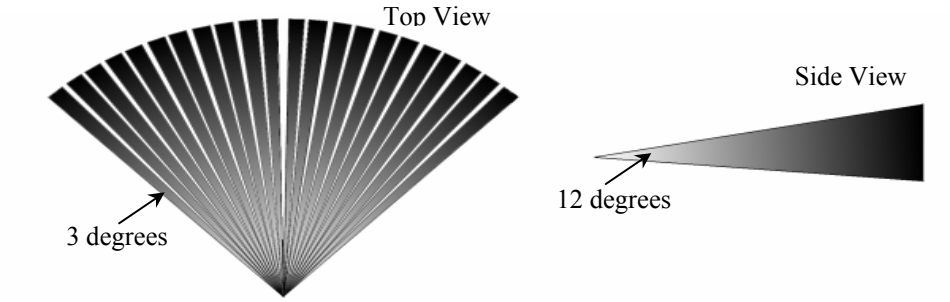

Fig. 4. Characteristic of field of view of Fresnal lens array. Each lens on the array creates two beams having a angular visibility of 3° separated by 1°.

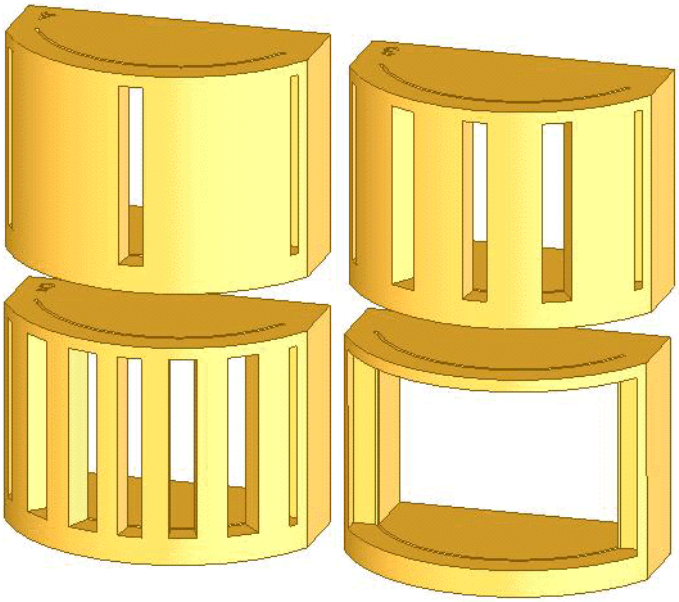

Fig. 5. Four different masks for selection of lens elements.

#9793 - $15.00 USD Received 30 November 2005; revised 17 January 2006; accepted 17 January 2006

Table 1. Summary of characteristics of Fresnel lens array

Parameter	Value
Angular coverage of each lens	7 ^{o}
Angular gap between adjacent beams	2 ^{o}
Angular gap between two beams from each lens	1 ^{o}
Lateral angular spread	12 ^{o}
Transmittance of lens in IR	75 %

3. Identification using Principal Components Regression and Multiple Hypothesis Testing

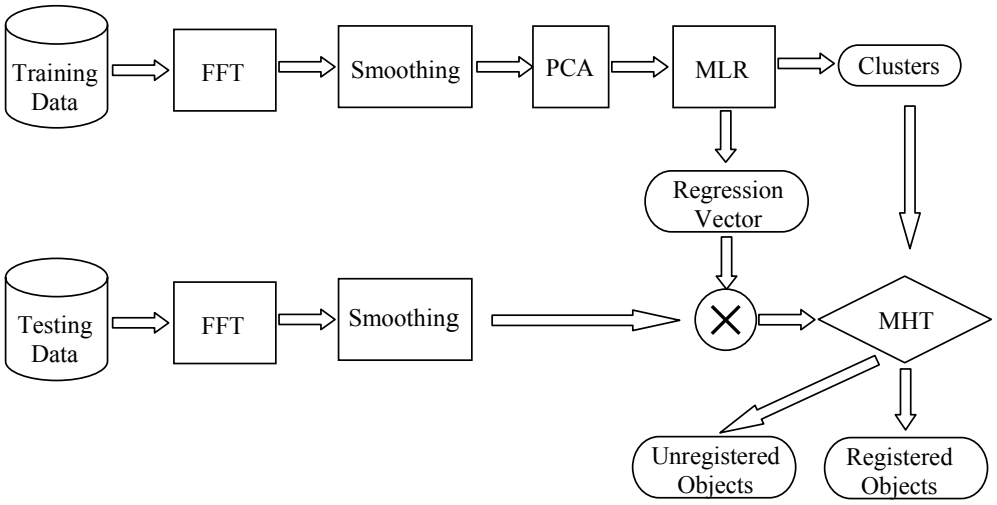

Fig. 6. The diagram of the proposed identification system.

Figure 6 outlines the identification process, both training and testing. We use Principal Components Regression (PCR) to find a regression vector F, such that the identity of a spectrum of unknown sensory data can be estimated, by an inner product of vector F and the spectrum *S*, i.e.,

$$I = S \bullet F \,. \tag{1}$$

PCR uses the full spectrum and is factor-based. The spectral information is not directly used in training, but is subject to factor analysis to find those factors that have the largest influence on data variations. PCR can be divided into two steps: principal components analysis (PCA) followed by standard multiple linear regression (MLR). In the multiple hypothesis testing (MHT), the identity of an unknown spectrum is estimated by Eq. (1) and then is checked against clusters and their distributions obtained from the training process.

3.1 Principal Components Analysis (PCA)

PCA is a spectral decomposition of the spectrum matrix S, retaining only those factors that have large singular values. The remaining factors associated with small singular values are

#9793 - $15.00 USD Received 30 November 2005; revised 17 January 2006; accepted 17 January 2006

assumed to be from noise, and therefore omitted from the later regression phase. The singular value decomposition (SVD) of a spectral matrix S can be represented by

$$S_{m\times n} = U_{m\times m}\Sigma_{m\times n}V^T_{n\times n}\,, \tag{2}$$

where the U and V are orthogonal matrices, m is the number of samples, n is the number of spectral points in one spectrum of the sensor's temporal signal.

$$\Sigma = \begin{bmatrix} \sigma_1 & & & & & & \\ & \sigma_2 & & & & & \\ & & \ldots & & & & \\ & & & \sigma_r & & & \\ & & & & 0 & & \\ & & & & & \ldots & \\ & & & & & & \ldots \\ & & & & & & 0 \end{bmatrix}. \tag{3}$$

Σ is diagonal with nonnegative singular values in descending order. Thus the spectrum matrix S can also be written as,

$$S = \sum_{i=1}^{r}\sigma_i u_i v_i^T = \sigma_1 u_1 v_1^T + \sigma_2 u_2 v_2^T + \ldots + \sigma_r u_r v_r^T\,. \tag{4}$$

S can be approximated by its first k singular values, assuming singular values for larger k are negligible.

$$\begin{aligned} S \approx S_k &= \sum_{i=1}^{k}\sigma_i u_i v_i^T \\ &= \sigma_1 u_1 v_1^T + \sigma_2 u_2 v_2^T + \ldots + \sigma_k u_k v_k^T\,, \\ &= \widetilde{U}_{m\times k}\widetilde{\Sigma}_{k\times k}\widetilde{V}^T_{k\times n} \end{aligned} \tag{5}$$

with $k \ll m, n$.

The spectrum matrix S also can be defined as

$$S \approx TP^T\,, \tag{6}$$

where

$T_{m\times k} = \widetilde{U}_{m\times k}\widetilde{\Sigma}_{k\times k}$,

$P = \widetilde{V}_{n\times k}$,

$SP = T$.

#9793 - $15.00 USD Received 30 November 2005; revised 17 January 2006; accepted 17 January 2006

T is the score matrix, and P is the factor matrix. Geometrically, P can be viewed as a new set of orthogonal coordinates spanning the inherent (true) dimensionality of the spectrum data matrix S, and T is the projection (scores) of S onto new coordinate system. For convenience, we will call it k-space.

3.2 Multiple Linear Regression (MLR)

Once we obtain the underlying factors and their corresponding scores, MLR is performed to regress those scores. In the classification process, the Fourier spectrum is first projected onto those factors obtained during training, and the resulting scores are correlated with the calibration vector obtained by MLR in k-space. We regress the spectrum vector against the score matrix $T_{m\times k}$, to get the regression vector $f_{k\times 1}$ in k-space, i.e., we find the least-squares solution of equation

$$I_{m\times 1} = T_{m\times k} f_{k\times 1} . \tag{7}$$

The least-squares solution for $f_{k\times 1}$ is

$$f_{k\times 1} = (T^T T)^{-1} T^T I = \tilde{\Sigma}^{-2} T^T I , \tag{8}$$

where

$$\tilde{\Sigma}^{-2} = \begin{bmatrix} \frac{1}{\sigma_1^2} & & & \\ & \frac{1}{\sigma_2^2} & & \\ & & \cdots & \\ & & & \frac{1}{\sigma_k^2} \end{bmatrix} . \tag{9}$$

Finally, from Eq. (6), Eq. (7), and Eq. (8) the regression vector can be written as follows

$$\begin{aligned} F_{n\times 1} &= P_{n\times k} f_{k\times 1} \\ &= P_{n\times k} \tilde{\Sigma}^{-2} T^T I \\ &= \tilde{V}_{n\times k} \tilde{\Sigma}^{-2} (\tilde{U}_{m\times k} \tilde{\Sigma}_{k\times k})^T I \\ &= \tilde{V}_{n\times k} \tilde{\Sigma}^{-1} \tilde{U}_{m\times k}^T I \end{aligned} \tag{10}$$

3.3 Multiple Hypothesis Testing

From multiple linear regression, we can obtain the resultant regression vector, as well as mean and covariance of clustered training data, $[\mu_1, \ldots, \mu_K]$ and $[\Sigma_1, \ldots, \Sigma_K]$, where K is the number of clusters. Therefore, for an unlabeled spectrum x, we will have K+1 hypothesis, $\{H_0, H_1, \ldots, H_K\}$, to test. The hypothesis H_0 represents "none". The decision rule then is

#9793 - $15.00 USD Received 30 November 2005; revised 17 January 2006; accepted 17 January 2006

$$x \in \begin{cases} H_0, & if \ \max_i \{p(x \mid H_i)\} < \gamma \\ H_i: \ i = \arg\max_i \{p(x \mid H_i)\}, & otherwise \end{cases} \tag{11}$$

where $p(x|H_i) = N(x|\mu_i, \Sigma_i)$ is the association of x with the i^{th} cluster and γ is a selected rejection threshold.

Recognition ability, of the process is measured by the false alarm rate, which can be defined by

$$FAR = \frac{\#\ of\ \ false\ sets}{\#\ of\ \ testing\ \ sets} \tag{12}$$

4. Experimental results

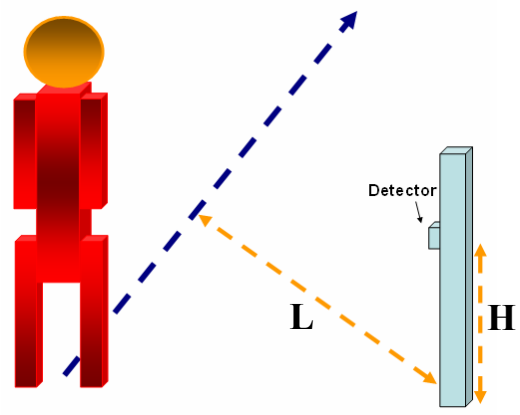

Fig. 7. An experimental setup for human identification. The center of the sensor element is perpendicular to the path.

The experimental setup is shown in Fig. 7. A sensor unit, which contains a pyroelectric IR sensor and a Fresnel lens array, is mounted on a pillar at a height of 80cm to detect the IR radiation from the target. The sensory data was collected when different people walked back and forth along a prescribed straight path, 2m or 3m away from and perpendicular to the sensor.

In response to heat flow, electric charge is built up on the sensing element by virtue of pyroelectric property. The electric charge results in an electric current which is converted to a voltage signal by a current to voltage transductance amplifier. Figure 8 shows temporal voltage signals generated by two different individuals walking across the field of view of the sensor. The corresponding Fourier spectra are shown in Fig. 9. It can be seen that the spectra generated by two people walking at a similar speed are different. On the other hand, for the same person, different speeds can also produce spectral differences and hence we need to take the effects of speed into account to build a functional identification system.

To find the optimal number of elements of a Fresnel lens array for classification, we modulated the visibility of pyroelectric sensors by Fresnel lens arrays with 1, 3, 5, and 11 transparent elements. The masks used for selection of different lens elements are shown in Fig. 5. We also studied the effects of the sensor location and sensor-target distance upon the identification performance. The sensor unit was located at the heights of 35cm, 80cm, and 120cm respectively and two fixed-paths, 2 m and 3 m from the sensor, were used. For each

#9793 - $15.00 USD Received 30 November 2005; revised 17 January 2006; accepted 17 January 2006

sensor-object configuration, 60 sets of data were collected for each person walking back and forth along a fixed-path at 3 different speed levels, namely fast, moderate, and slow, all within the range of the daily walking habit. The Fourier spectra of measured signals of two human objects are displayed in Fig. 10. Each column displays the data collected at the different walking speeds. Each row displays the data obtained with the different element numbers of Fresnel lens arrays. Each subfigure contains 20 superimposed data sets which were gathered from 20 independent walks. It can be seen from the degree of spectra overlap that the repeatability of the spectral features is high.

The identification procedure consists of two parts: training and testing. During training, we clustered all 120 data sets from each sensor-lens pair into 6 clusters, two persons and three speeds. Since we know the label of each data set, the clustering process can be viewed as supervised training. As such, we can map these 6 clusters to 6 points equally distributed along a circle using linear regression. The resultant regression vector obtained from PCR defines the linear boundary between the data sets.

Figure 11(a)-(c) show the clustering results for the sensor units with 1, 5, and 11-element Fresnel lens arrays. The results show that the use of an increased number of lens elements in the lens array can yield better performance in the supervised classification. Figure 11(d) shows the contours of probability density distributions (pdfs) associated with the clusters in Fig. 11(c). Contours of probability density ranging from 0.1 to 0.7 are drawn in Fig. 11(d) to aid in interpretation. After determining the optimal number of lens element, we studied the effects of sensor locations. Figure 12 and Fig. 13 show the clustering results and their pdfs for the sensor unit with an 11-element lens array placed at the heights of 120cm and 35cm respectively.

#9793 - $15.00 USD Received 30 November 2005; revised 17 January 2006; accepted 17 January 2006

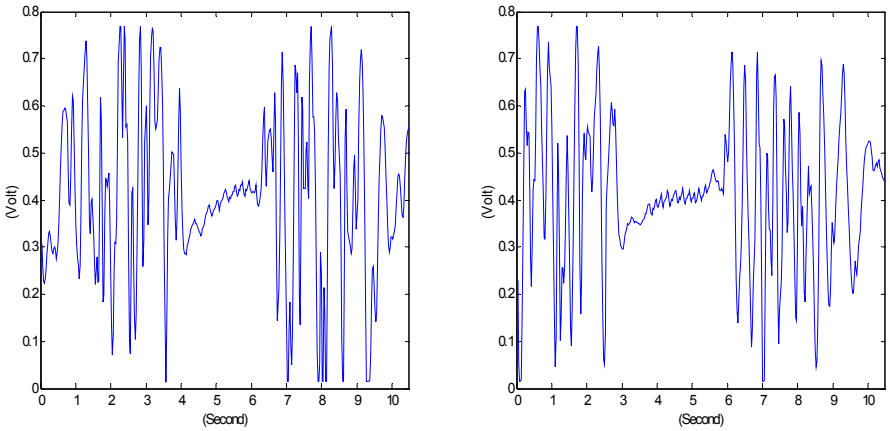

Fig. 8. Output signals for two different individuals walking across the field of view of one sensor unit.

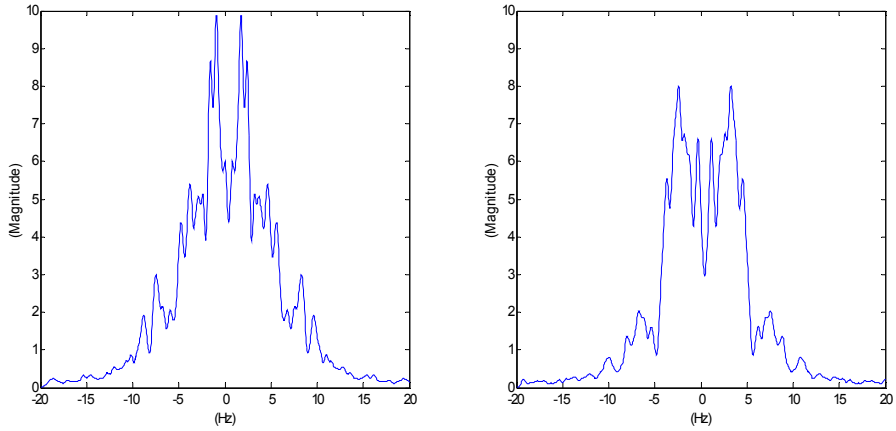

Fig. 9. The spectra for two different individuals by performing the Fourier transform of the temporal signals in Fig. 8.

#9793 - $15.00 USD Received 30 November 2005; revised 17 January 2006; accepted 17 January 2006

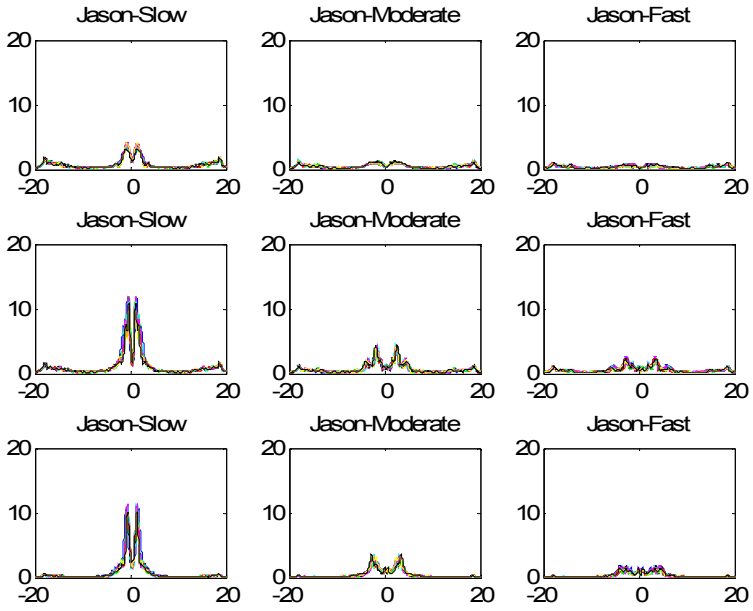

(a)

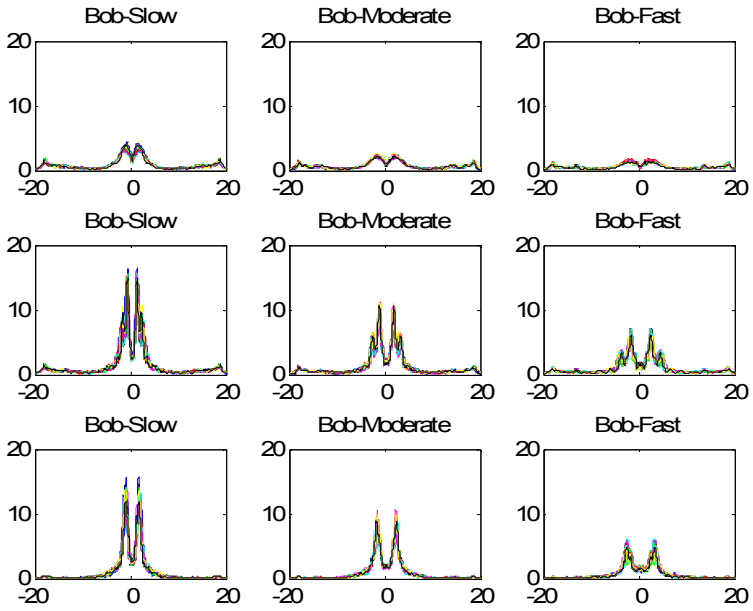

(b)

Fig. 10. Each column is for different speed levels (fast, moderate, and slow, respectively). Each row is for different element numbers of Fresnel lens arrays (1, 5, and 11, respectively). Each subfigure contains 20 superimposed data sets which were gathered from 20 independent walks at the same speed. (a) The data sets of Jason. (a) The data sets of Bob.

#9793 - $15.00 USD Received 30 November 2005; revised 17 January 2006; accepted 17 January 2006

We also carried out multiple hypothesis testing (MHT) for human identification. 20 data sets were collected for each person walking at random speeds. For the two registered persons, there are 40 data sets for each configuration of sensor units. We calculate the probability density of each data set to determine its cluster membership. The threshold for membership was chosen to be 0.05. If the probability density value of a data set is below the threshold, the data set will be labeled as others.

Figure 14 shows the results for the sensor unit with an 11-element Frsnel lens array at 3 different heights. In each subfigure, the left histogram is generated from 20 data sets with Jason as the subject, whereas the right histogram is generated from data with Bob as the subject. Figure 15 shows the testing results at 3 different heights with a sensor-object distance of 3m. The false alarm rates for different sensor configuration are summarized in Table 2. It can be seen that the sensor unit with an 11-element lens array located at the height of 80cm displays the best performance.

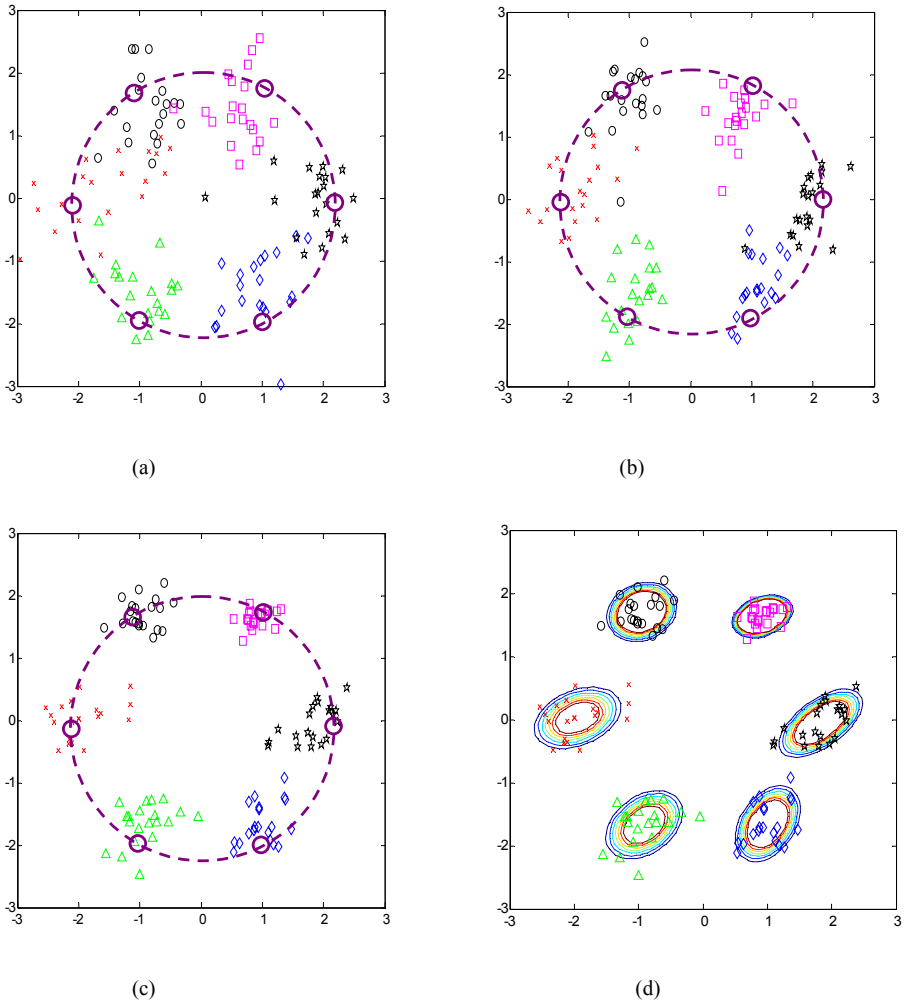

Fig. 11. The supervised clustering results upon 6 labels for 120 data sets collected from the sensor unit placed at the height of 80 cm. (a) Data from the sensor unit with the 1-element Fresnel lens array. (b) Data from the sensor unit with the 5-element Fresnel lens array. (c) Data from the sensor unit with the 11-element Fresnel lens array. (d) Probability density distributions of the clusters in (c).

#9793 - $15.00 USD Received 30 November 2005; revised 17 January 2006; accepted 17 January 2006

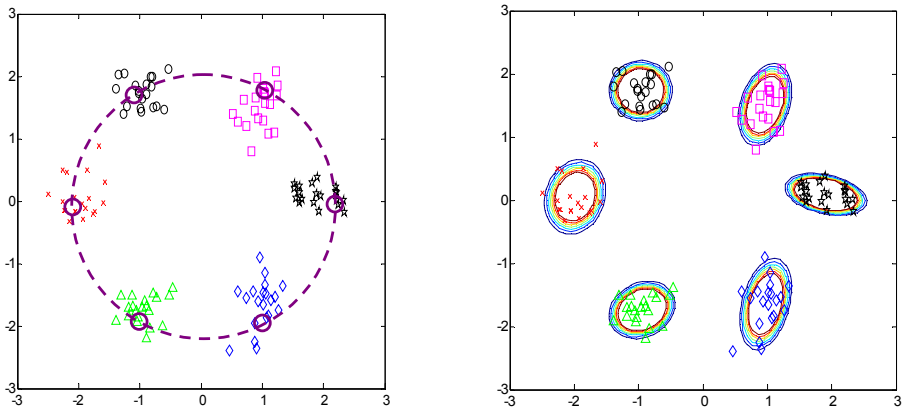

(a) (b)

Fig. 12. The clustering results for 120 data sets from the sensor unit placed at the height of 120 cm. (a) Data from the sensor unit with the 11-element Fresnel lens array. (b) Probability density distributions of the clusters.

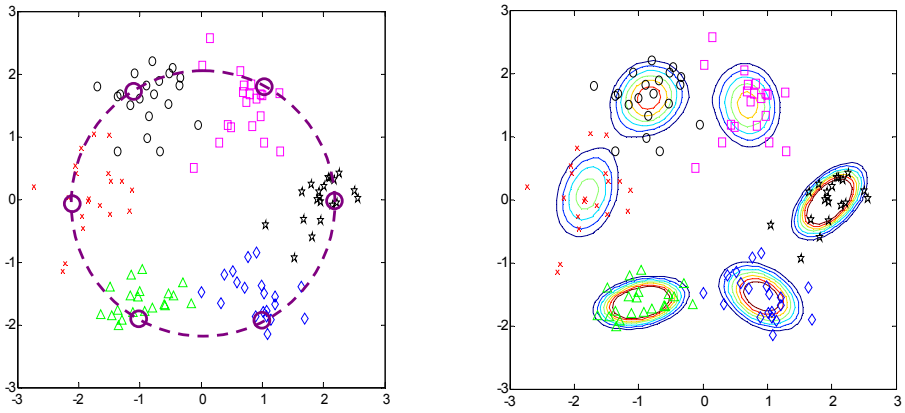

(a) (b)

Fig. 13. The clustering results for 120 data sets from the sensor unit placed at the height of 35 cm. (a) Data from the sensor unit with the 11 Fresnel lens array. (b) Probability density distributions of the clusters.

#9793 - $15.00 USD Received 30 November 2005; revised 17 January 2006; accepted 17 January 2006

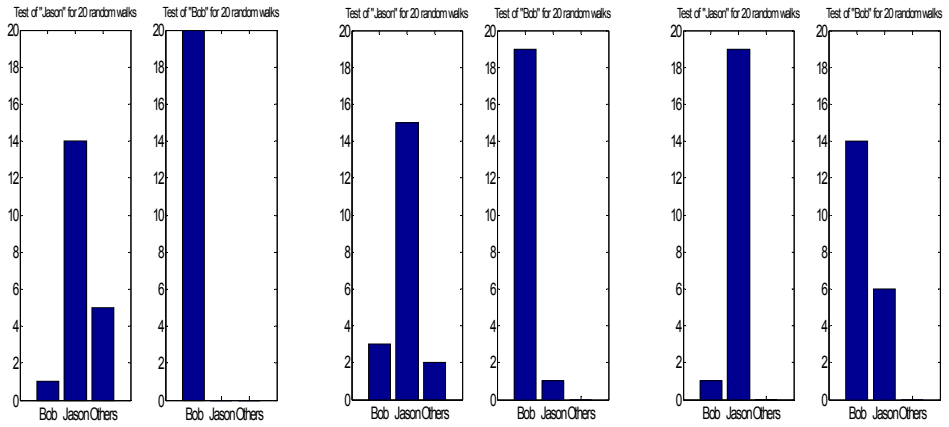

(a) (b) (c)

Fig. 14. The identification results for a sensor unit with an 11-element lens array at the sensor-object distance of 2m. (a) The sensor unit is placed at the height of 120 cm. (b) The sensor unit is placed at the height of 80 cm. (c) The sensor unit is placed at the height of 35 cm.

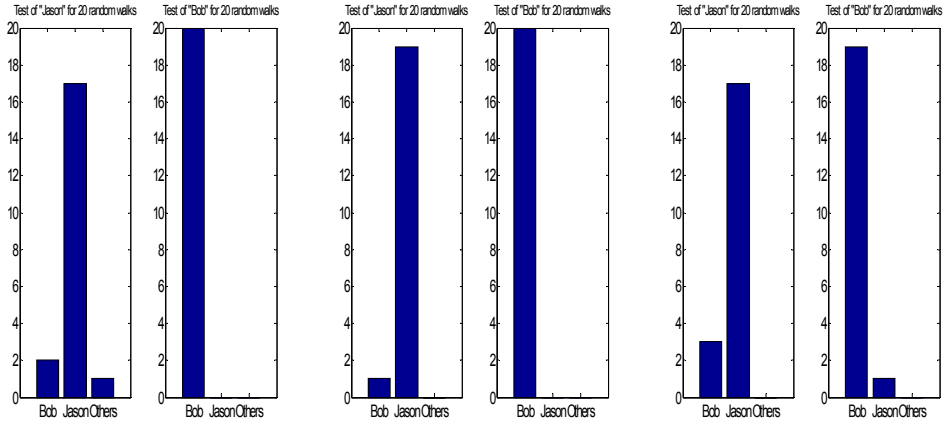

(a) (b) (c)

Fig. 15. The identification results for a sensor unit with the 11-element lens array at the sensor-object distance of 3m. (a) The sensor unit is placed at the height of 120 cm. (b) The sensor unit is placed at the height of 80 cm. (c) The sensor unit is placed at the height of 35 cm.

Table 2. Summary of identification false alarm rates with different sensor configurations.

H	**35 cm**		**80 cm**		**120 cm**	
N \ *L*	**2 m**	**3 m**	**2 m**	**3 m**	**2 m**	**3 m**
1	17.5 %	17.5 %	20 %	12.5 %	45 %	17.5 %
3	20 %	12.5 %	20 %	7.5 %	32.5 %	17.5 %
5	17.5 %	12.5 %	17.5 %	5 %	35 %	10 %
11	17.5 %	10 %	15 %	2.5 %	15 %	7.5 %

H: Height of sensor unit; *L*: Sensor-object distance; *N*: Number of lens elements

#9793 - $15.00 USD Received 30 November 2005; revised 17 January 2006; accepted 17 January 2006

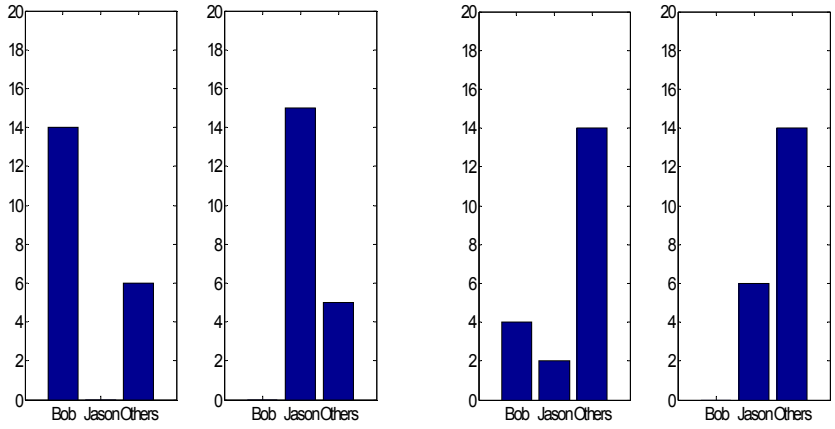

Fig. 16. The identification results for the registered objects and unregistered objects at the same rejection threshold. (a) Recognition results for two registered objects: Bob and Jason. (b) Rejection results for two unregistered objects.

Figure 16 shows the testing results using sensor unit with 11-element lens array located at a height of 80 cm and at a range of 3 m. We used a rejection threshold, γ, of 0.1 resulting in recognition and rejection rates greater than 70 percent.

5. Conclusion

In this paper, we introduce the concept and an initial design of a novel human recognition system based on a pyroelectric infrared (PIR) sensor. The spectral content of the sensor's temporal signal, generated by humans walking along a fixed-path, is used to represent the human motion features. In the training phase, features at three levels of speeds are collected. Despite the simplicity of the supervised training method we used, the testing results are able to discriminate between two registered humans and reject other unregistered humans. Generally speaking, human motion is not very distinctive, but we find here that it is sufficiently discriminatory to allow identification among a small group of humans.

By employing a sensor array, or multiple sensor nodes, and additional feature representations, the system robustness could be improved. With more advanced signal processing and feature extraction techniques, we might develop a path-independent human recognition system, which is also less sensitive to the walking speed of objects. Research in this direction is underway in our laboratory.

Acknowledgments

The authors would like to express their gratitude to Steve Feller and John Burchett for assisting with the experimental setup and acknowledge the support of the Army Research Office through the grant DAAD 19-03-1-03552.

#9793 - $15.00 USD Received 30 November 2005; revised 17 January 2006; accepted 17 January 2006